

Single Particle Analysis of Secondary Organic Aerosols Formed from 1,4-Cyclohexadiene Ozonolysis Using a Laser-Ionization Single-Particle Aerosol Mass Spectrometer

Masahiro Narukawa,[1,†] Yutaka Matsumi,*[1] Jun Matsumoto,[1,††] Kenshi Takahashi,[1,†††] Akihiro Yabushita,[2,††††] Kei Sato,[3] and Takashi Imamura[3]

[1]Solar-Terrestrial Environment Laboratory, Nagoya University, 3-13 Honohara, Toyokawa 442-8507

[2]Horiba, Ltd., 2 Miyanohigashi, Kisshoin, Minami, Kyoto 601-8510

[3]National Institute for Environmental Studies, 16-2 Onogawa, Tsukuba 305-8506

Received March 27, 2007; E-mail: matsumi@stelab.nagoya-u.ac.jp

Real-time analysis of secondary organic aerosol (SOA) particles formed from 1,4-cyclohexadiene (CHD) ozonolysis in a smog chamber was performed using a laser-ionization single-particle aerosol mass spectrometer (LISPA-MS). The instrument can be used to obtain both the size and chemical compositions of individual aerosol particles with a high time-resolution (≈2 s at the maximum). Both positive- and negative-ion mass spectra can be obtained by changing the voltage polarity of the instrument. The negative-ion spectra of the SOA particles provided important information about the chemical compositions of the SOA particles. In the negative-ion spectra, intense mass peaks were determined to correspond to ions with carboxyl and aldehyde groups. The signal intensities of the intense mass peaks from compounds with carboxyl groups were higher than those from compounds with aldehyde groups as a function of the particle size. The peaks suggest that the SOA particles contain more oxygenated organic compounds as the particle size increases, namely, the chemical compositions of the SOA particles vary as a function of the particle size. We demonstrated that the real-time single-particle analysis of SOA particles by using the LISPA-MS technique can be used to clarify the formation and transformation processes of SOA particles in smog chambers.

Organic compounds account for a large, sometimes even dominant, fraction of the particulate matter in the air. They influence the chemical and physical properties of aerosol particles and thus have effects on the atmosphere and climate through interaction with reactive trace gases, water vapor, clouds, precipitation, and radiation. Several scientific papers have reviewed organic aerosol chemistry and physics in the atmosphere.[1–6] The source of the main fraction of the organic aerosols is of secondary origin;[5] in other words, most organic aerosol components are chemically formed in the atmosphere. The chemistry of secondary organic aerosol (SOA) formation and transformation processes has been studied using smog chambers.[4] Chemical compositions of SOA particles formed in chambers have been studied using off-line techniques, which have provided important information about the chemical compositions of SOA particles. However, the off-line techniques are time-consuming and tend to have sampling artifacts.[2] In addition, it is difficult to measure the size and chemical compositions of individual SOA particles simultaneously and in real time by using the off-line techniques.

Real-time aerosol mass spectrometry has been developing since the mid 1990s. Most of the instruments can determine the size and count, and analyze the mass of individual particle constituents online with high time-resolution. The chemistry of SOA particles has been studied using such instruments. For example, by using an aerosol time-of-flight mass spectrometer (ATOFMS), real-time detection of oligomers in SOA particles formed from photooxidation of 1,3,5-trimethylbenzene and NO_x has been reported.[7] The role of organic peroxides in SOA formation for reactions of monoterpenes with O_3 has been elucidated using a thermal desorption particle beam mass spectrometer (TDPBMS).[8] The direct polymerization of isoprene and α-pinene on acidic aerosols has been studied using an aerosol mass spectrometer (AMS).[9] Reviews of real-time aerosol mass spectrometry are available in the literature.[10,11]

We have recently developed a laser-ionization single-particle aerosol mass spectrometer (LISPA-MS) for real-time single-particle measurements.[12–14] The LISPA-MS is capable of high time-resolution measurements to determine the size and chemical compositions of individual particles. Either positive- or negative-ion mass spectra can be obtained for individual particles by changing the voltage polarity of the instrument. Apparent changes in the chemical compositions of Asian

† Present address: Heat and Fluid Dynamics Department, Research Laboratory, IHI Corporation, 1 Shin-Nakahara-cho, Isogo, Yokohama 235-8501

†† Present address: Integrated Research Institute, Tokyo Institute of Technology, 4259 Nagatsuta, Midori-ku, Yokohama 226-8503

††† Present address: Pioneering Research Unit for Next Generation, Kyoto University, Gokasho, Uji, Kyoto 611-0011

†††† Present address: Department of Molecular Engineering, Graduate School of Engineering, Kyoto University, Kyoto 615-8510

Published on the web January 10, 2008; doi:10.1246/bcsj.81.120

dust particles transported from the Asian continent to Japan have been observed by using the LISPA-MS.[12] By measuring the standard aerosol particles of dicarboxylic acids and SOA particles formed from cyclohexene ozonolysis using the LISPA-MS, it has been found that the negative-ion mass spectra provide information about the molecular weights of the organic compounds in the particles.[13]

Here, we present an application of the LISPA-MS to the study of SOA particles formed in a smog chamber. The size and chemical compositions of the SOA particles formed from 1,4-cyclohexadiene (CHD) ozonolysis were analyzed using the LISPA-MS. CHD is a hydrocarbon containing two symmetric non-conjugated double bonds in the six-membered ring, and a simple surrogate of γ-terpinene that is emitted to the atmosphere as a biogenic hydrocarbon. The purposes of this paper were to better understand the formation and transformation processes of single SOA particles by using real-time measurements and to demonstrate the ability of the LISPA-MS.

Experimental

Laser-Ionization Single-Particle Aerosol Mass Spectrometer (LISPA-MS). Although the details of the LISPA-MS have been described in the literature,[13] we briefly describe the LISPA-MS. A schematic diagram of the particle inlet and the ion source region of the LISPA-MS is shown in Fig. 1a. Aerosol particles are introduced into an aerodynamic lens through a flow-limiting molybdenum orifice with a diameter of 300 μm. In the reduced pressure region, particles are horizontally focused into a narrow particle beam (≈1 mm diameter) in the center of the gas flow by the aerodynamic lens.[15] After exiting the lens, the particle beam is transmitted into the ion source region through differentially pumped stages with two skimmers (Precision Instrument

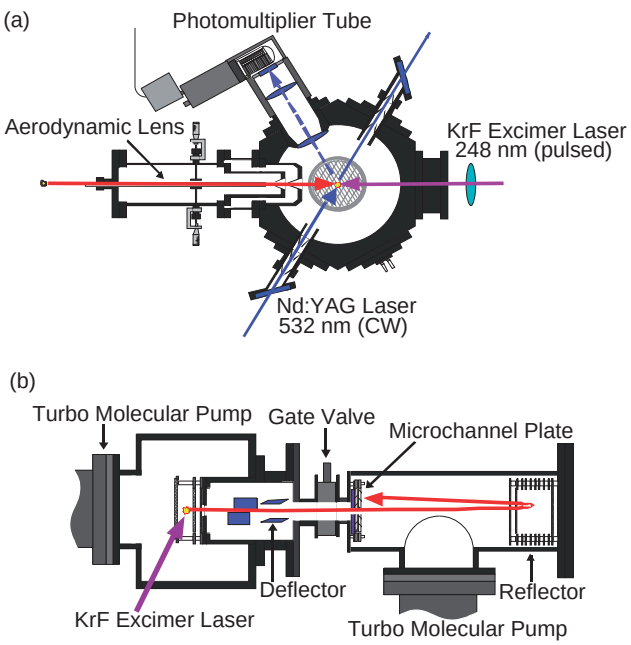

Fig. 1. Diagrams of (a) the particle inlet and the ion source region of the laser-ionization single-particle aerosol mass spectrometer (LISPA-MS) and (b) the ion source region and reflectron time-of-flight mass spectrometer of the LISPA-MS.

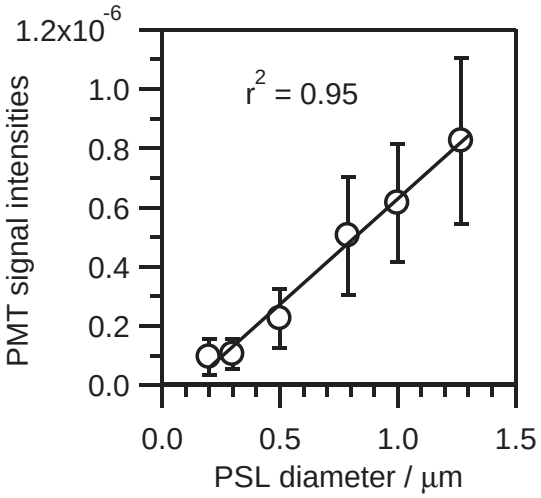

Fig. 2. PMT signal intensities of YAG laser scattered light as a function of polystyrene latex (PSL) particle diameter. The vertical bars show two-standard deviations (2σ) for the averaged data. The correlation coefficient ($r^2 = 0.95$) is calculated from the weighted regression line by the size of the error bars.

Services).

For detecting the particles introduced into the ion source region, a continuous-wave laser beam, produced using a frequency-doubled Nd:YAG laser at 532 nm, crosses the particle beam as shown in Fig. 1a. The scattered light from the individual particles at 532 nm is detected by a photomultiplier tube (PMT, Hamamatsu, 1P28A). The intensity of the scattered light is approximately proportional to the particle size and is utilized for roughly determining the particle size. Particle size calibration of the LISPA-MS is performed by sampling dry polystyrene latex particles (Duke Scientific and JSP). Figure 2 shows the PMT signal intensities of YAG laser scattered light as a function of polystyrene latex particle diameter. The correlation coefficient ($r^2 = 0.95$) in Fig. 2 is calculated from the weighted regression line. The detection efficiency for particles smaller than the wavelength of the detection laser light is very low due to Mie scattering. Thus, the lower limit of the detected particle diameter is ≈200 nm. The signals from the PMT are amplified and discriminated, and those above a selectable threshold level trigger desorption/ionization laser pulses. A pulsed KrF excimer laser at 248 nm (Lambda Physik, OPTex) is used as a light source for the desorption/ionization of particles.

A diagram of the ion source region and reflectron time-of-flight mass spectrometer of the LISPA-MS is shown in Fig. 1b. The resultant ions are accelerated from the ion source region to the reflector assembly and are then detected by a microchannel plate detector (MCP, Hamamatsu). By monitoring the ion current from the MCP as a function of time, a complete mass spectrum is obtained for the chemical compositions of a single particle. The ion signals from the detector are amplified linearly, digitized, and recorded as mass spectra with a high time-resolution (≈2 s at the maximum). Positive or negative-ion mass spectra are obtained for individual particles by changing the voltage polarity of the ion source region and the TOF-MS.

Smog Chamber Experiments. Laboratory studies were conducted by using an indoor evacuable and bakable photochemical smog chamber at National Institute for Environmental Studies

Table 1. Initial Conditions for 1,4-Cyclohexadiene (CHD) Ozonolysis in the NIES Smog Chamber

Run No.	P_0/Torr	T_0/K	$[CHD]_0$/ppmv	$[O_3]_0$/ppmv
1	763	298	2.09	1.93
2	773	297	2.07	1.99
3	771	298	2.06	2.01
4	771	298	2.07	1.98

(NIES). The chamber was a stainless steel cylinder having a volume of 6.065 m^3, a length of 3500 mm and an inner diameter of 1450 mm. The inner surface of the chamber was Teflon-coated (tetrafluoroethylene–perfluoroalkyl vinyl ether copolymer). The details of the NIES smog chamber have been described in the literature.[16]

The NIES smog chamber was filled with 760 Torr of dry purified air prior to introducing the reactants. Ozone was introduced into the chamber from an ozone generator (Iwasaki, OP-20W). The reaction was started following the introduction of 1,4-cyclohexadiene (CHD; 96% purity, Wako Pure Chemical Industries), which was used without further purification. The initial conditions for each run of the CHD ozonolysis are given in Table 1. The reactant mixture was stirred well with a mixing fan for a few minutes, after introducing CHD into the chamber. Each run was performed in the dark under dry conditions (relative humidity < 1 ppmv) without any seed particles or hydroxyl radical scavengers and was typically terminated within ≈60 min. During each run, the SOA particles formed in the chamber were sampled through a stainless steel tube that was 0.635 cm (0.25 inches) in diameter and ≈3 m in length and were directly introduced to the LISPA-MS. The concentrations of the gaseous reactants were measured every 6 min with a FT-IR spectrometer (Nicolet, Nexus 670) equipped with a liquid N_2-cooled MCT detector. The spectral resolution was 1.0 cm^{-1}. The spectrometer was coupled to a white mirror system (base path 1700 mm), which was operated at 130 traverses, giving a total absorption path length of 221.5 m, including the transfer path. The size distribution and the number concentrations of the SOA particles were measured on a scanning mobility particle sizer instrument (SMPS; TSI, Model 3934), which consists of an electrostatic classifier (TSI, Model 3071A) and a condensation particle counter (CPC; TSI, Model 3025A). The details of SOA formation studies by using the NIES smog chamber are described in the literature.[17,18]

Results and Discussion

Ozonolysis of 1,4-Cyclohexadiene (CHD). As a representative example, temporal profiles of the concentrations (ppmv) of CHD and O_3 from CHD ozonolysis for Run No. 3 are shown in Fig. 3. The concentrations of the reactants decreased immediately after mixing the reactants in the chamber. A temporal profile of the mass concentrations (mg m^{-3}) of the SOA particles for Run No. 3 is also shown in Fig. 3. The SOA mass concentrations were calculated from the electrical mobility diameter of the particles, assuming a spherical shape and a density of 1.4 g cm^{-3}, which was determined from the particulate products of cyclohexene ozonolysis.[19] The mass concentrations were also corrected for wall loss.[17] The SOA particles grew to the detectable size (≳200 nm) of the LISPA-MS over a few minutes after the reactants were mixed. The SOA mass concentrations remarkably increased within ≈15 min from the start of the reaction, followed by a little increase, as shown in Fig. 3.

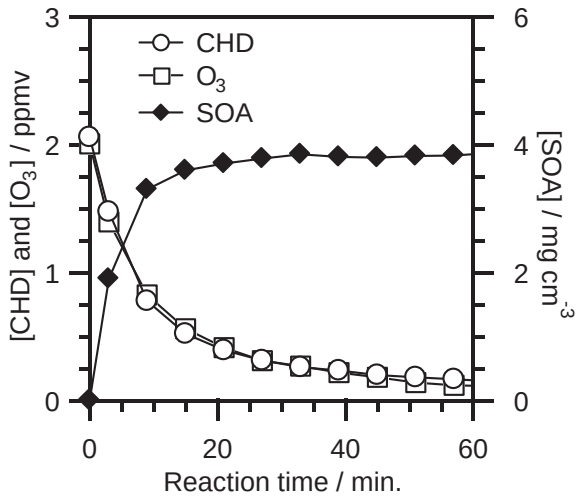

Fig. 3. Temporal profile of the concentrations of 1,4-cyclohexadiene (CHD) (○), ozone (□), and secondary organic aerosol (SOA) mass (◆) in CHD ozonolysis (Run No. 3) conducted in the NIES smog chamber.

CHD has two double bonds; hence, one molecule of CHD can react with two molecules of O_3. The concentration of O_3 should decrease more quickly than that of CHD. However, as seen in Fig. 3, CHD was consumed in a one-to-one reaction with O_3. In cycloalkene ozonolyses, hydroxyl radical (OH) formation in the gas-phase in excellent yields has been reported.[20] Without OH scavengers in cycloalkene ozonolyses, the concentrations of cycloalkenes decreases more quickly than those of O_3,[21,22] that is, a part of the cycloalkenes is consumed by reactions with OH. CHD ozonolysis can form OH as well, which undergoes subsequent reactions with CHD. Therefore, CHD can react with both O_3 and OH. The depletion rate of CHD in our present study can be expressed as

$$-\frac{\mathrm{d[CHD]}}{\mathrm{d}t} = k_1[\mathrm{CHD}][\mathrm{O_3}] + k_2[\mathrm{CHD}][\mathrm{OH}], \quad (1)$$

where k_1 and k_2 are the rate constants for the gas-phase reactions of CHD with O_3 and OH, respectively. The values of k_1 and k_2 at 298 K have been reported to be 4.6×10^{-17} and 9.95×10^{-11} cm^3 $molecule^{-1}$ s^{-1}, respectively.[23,24] Integrating and rearranging Eq. 1, we derived the following equation:[25]

$$\ln\left(\frac{[\mathrm{CHD}]_t}{[\mathrm{CHD}]_0}\right) + k_1 \int_0^t [\mathrm{O_3}]\mathrm{d}t = -k_2[\mathrm{OH}]_{\mathrm{av}}t, \quad (2)$$

where $[OH]_{av}$ is the average concentration of OH radicals, which react with CHD between $t = 0$ and t. Using the values of k_1 and k_2 and the measured concentrations of CHD and O_3, we could calculate the OH concentration by using Eq. 2.[25,26] The average concentration of OH within the reaction time was estimated to be ≈2×10^6 molecule cm^{-3} (≈0.1 pptv), suggesting that the concentrations of OH is about six orders of magnitude lower than those of O_3. On the other hand, the rate constant of the reaction of CHD with OH is six orders of magnitude higher than that with O_3. Thus, OH should consume the same amount of CHD as consumed by O_3.

As an example of the reactions in the CHD ozonolysis, a reaction pathway that forms malonic acid (MW 104), the ion

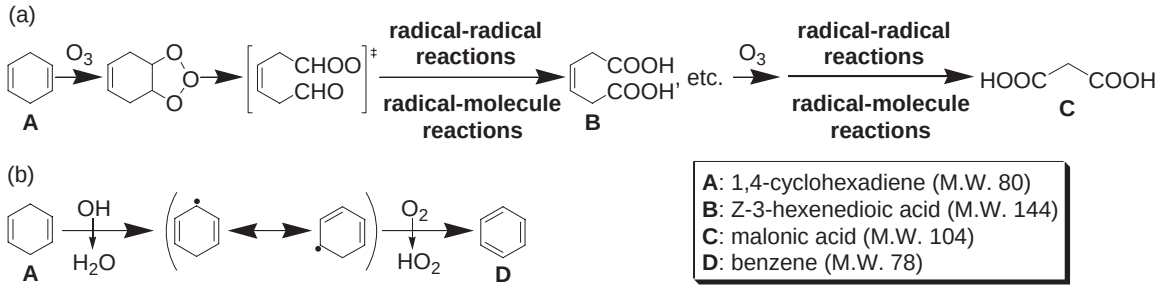

Fig. 4. (a) Formation pathway for malonic acid (MW 104) during CHD ozonolysis. The double dagger ‡ denotes an energy-rich Criegee intermediate. (b) Formation pathway for benzene during reaction of CHD with OH.

peak at $m/z = 103$, which corresponds to that which appeared as a strong peak in the negative-ion mass spectra of the SOA particles from CHD ozonolysis, as discussed later, is shown in Fig. 4a. CHD has two symmetric non-conjugated double bonds in the six-membered ring, so that O_3 attacks a double bond of CHD, leading to an energy-rich Criegee intermediate.[24] Further reactions involving the intermediate afford *Z*-3-hexenedioic acid (MW 144), which is a product of the first ozonolysis. Ozone also attacks the double bond of *Z*-3-hexenedioic acid, followed by other reactions, to give malonic acid, as shown in Fig. 4a. As a result, organic compounds with two functional groups (aldehyde and/or carboxyl groups), such as malonic acid, are expected to be the major products in CHD ozonolysis. In addition, OH can attack CHD as discussed above. As an example of the reactions of CHD with OH, a reaction pathway that forms benzene is shown in Fig. 4b. Benzene is a major gaseous product in the reactions of CHD with OH.[27] Thus, the products formed from the reactions of CHD with O_3 and OH should be a part of the SOA particles.

Mass Spectra of SOA Particles Measured by the LISPA-MS. Figure 5 shows positive-ion (Run No. 2, detected at 30.7 min after the reaction start) and negative-ion (Run No. 1, 59.5 min) mass spectra of the SOA particles. In the positive-ion mass spectra of the SOA particles formed during CHD ozonolysis, the mass peaks at $m/z = 39$ and 43 were dominant, as shown in Fig. 5a. The ions at $m/z = 39$ and 43 were assigned to be $C_3H_3^+$, and $C_3H_7^+$ and/or CH_3CO^+, respectively, which are obviously fragment ions. This result is consistent with those from our previous study.[13] In our previous study,[13] the standard aerosol particles of dicarboxylic acids and SOA particles formed from cyclohexene ozonolysis have been analyzed using the LISPA-MS, and we have found that the intense mass peaks in the positive-ion spectra of those particles consist of fragment ions, and not molecular and molecular-related ions.

In the negative-ion mass spectra of the SOA particles formed from the CHD ozonolysis, a strong mass peak at $m/z = 103$ appeared, as shown in Fig. 5b. The ion at $m/z = 103$ can be formed by proton elimination from malonic acid (MW 104), which is easily formed from CHD ozonolysis, as shown in Fig. 4a. In our previous study,[13] we have also found that molecular-related ions $[M - H]^-$ are observed with relatively strong intensities in the negative-ion spectra of standard aerosol particles of dicarboxylic acids, including malonic acid. It has also been found that the ions, which appeared as strong mass peaks in the negative-ion spectra of SOA particles

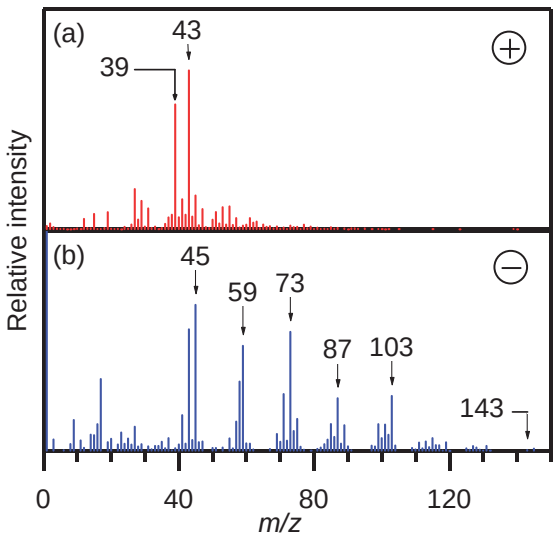

Fig. 5. Representative mass spectra obtained from each single SOA particle formed from CHD ozonolysis: (a) positive ion (Run No. 2, detected at 30.7 min after the reaction start) and (b) negative ion (Run No. 1, 59.5 min).

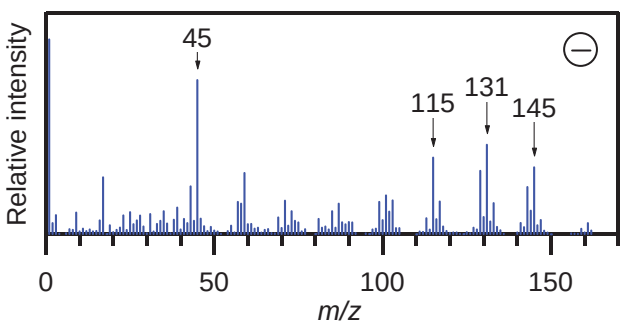

Fig. 6. Representative negative-ion mass spectrum obtained from a single SOA particle formed from cyclohexene ozonolysis.

formed from cyclohexene ozonolysis, consist of the molecular-related ions $[M - H]^-$ of the reaction products and fragment ions,[13] as shown in the negative-ion spectrum of the SOA particles formed from the cyclohexene ozonolysis in Fig. 6. Thus, the strong mass peak at $m/z = 103$ in the negative-ion spectra from CHD ozonolysis should correspond to malonic acid. It is likely that strong mass peaks in the negative-ion spectra from the CHD ozonolysis correspond to molecular-related ions $[M - H]^-$ of the reaction products

Table 2. Intense Mass Peaks (m/z) in Negative-Ion Mass Spectra and Corresponding Ions

m/z	Ions
43	CH_3CO^-
45	$HCOO^-$
59	CH_3COO^-
71	$OHCCH_2CO^-$ and/or $C_3H_7CO^-$
73	$OHCCOO^-$ and/or $C_2H_5COO^-$
87	$OHCCH_2COO^-$ and/or $C_3H_7COO^-$
103	$HOOCCH_2COO^-$

and fragment ions as well. Therefore, the negative-ion mass spectra provide important information for investigating the SOA formation processes in CHD ozonolysis.

In the negative-ion mass spectra from cyclohexene ozonolysis, the ion peak at $m/z = 145$, which corresponds to adipic acid (MW 146) that is formed via ozonolysis, was intense, as shown in Fig. 6. On the other hand, in the negative-ion spectra from CHD ozonolysis, the ion peak at $m/z = 103$, corresponding to malonic acid was intense, whereas the ion peak at $m/z = 143$, corresponding to *Z*-3-hexenedioic acid (MW 144), which is formed via the first ozonolysis as shown in Fig. 4a, was weak, as shown in Fig. 5b. The strong mass peak at $m/z = 103$ and the weak one at $m/z = 143$ suggest that the second ozonolysis in the CHD ozonolysis is rapid; namely, the products of the first ozonolysis are quickly consumed by O_3 and/or OH.

The strong mass peaks at $m/z = 45$, 59, 73, 87, and 103 in the negative-ion mass spectra from CHD ozonolysis have also been observed in the negative-ion spectra from cyclohexene ozonolysis, as shown in Fig. 6.[13] The compounds, which correspond to those strong mass peaks in the negative-ion spectra from cyclohexene ozonolysis, have been explained to be oxygenated organic compounds with aldehyde and carboxyl groups.[13] Thus, the strong peaks in the negative-ion spectra from CHD ozonolysis can also be interpreted as being due to oxygenated organic compounds with aldehyde and carboxyl groups. Table 2 lists the intense mass peaks, which appeared in the negative-ion spectra from the CHD ozonolysis, and the corresponding ions. The ions corresponding to the peaks at $m/z = 45$ and 59 are $HCOO^-$ and CH_3COO^-, respectively, and the ions corresponding to the peaks at $m/z = 73$ and 87 are $OHCCOO^-$ and/or $C_2H_5COO^-$, and $OHCCH_2COO^-$ and/or $C_3H_7COO^-$, respectively. Accordingly, it is suggested that all of these ions are directly and/or indirectly formed via proton elimination of the compounds with carboxyl groups. On the other hand, the ion corresponding to the peak at $m/z = 43$ is CH_3CO^-, and the ions corresponding to the peak at $m/z = 71$ are $OHCCH_2CO^-$ and/or $C_3H_7CO^-$. Similarly, it is suggested that these ions are directly and/or indirectly formed via proton elimination of the compounds with aldehyde groups.

Size Dependence of Negative-Ion Mass Spectra of SOA Particles. Distributions of the ion signal intensities in the negative-ion mass spectra from the CHD ozonolysis changed as a function of the particle size, which was roughly determined from the scattered light intensity of the SOA particles, as shown in Fig. 2. Figure 7 shows averaged negative-ion spectra, in which (a) the 40 smallest particles were averaged and their mean diameter was 0.3 μm, and (b) the 40 largest particles were averaged and their mean diameter was 2.1 μm. Data obtained from all of the experiments (Run Nos. 1–4) were combined and averaged. The signal intensity ratios in the range of m/z from 45 to 43 and from 73 to 71 in the negative-ion spectra generally changed with the particle size, as shown in Fig. 7. It is thought that the peaks at $m/z = 43$ and 71 correspond to compounds with aldehyde groups, whereas the peaks at $m/z = 45$ and 73 correspond to compounds with carboxyl groups, as discussed above. The carboxyl group can form from the oxidation of an aldehyde group. Therefore, the differences in the signal intensity ratios observed in the negative-ion spectra imply that the SOA particles with relatively high signal intensity ratios consist of the products formed from more progressed oxidation reactions than those with relatively low signal intensity ratios, whereas the absolute ionization response of those compounds in the instrument have not been determined.

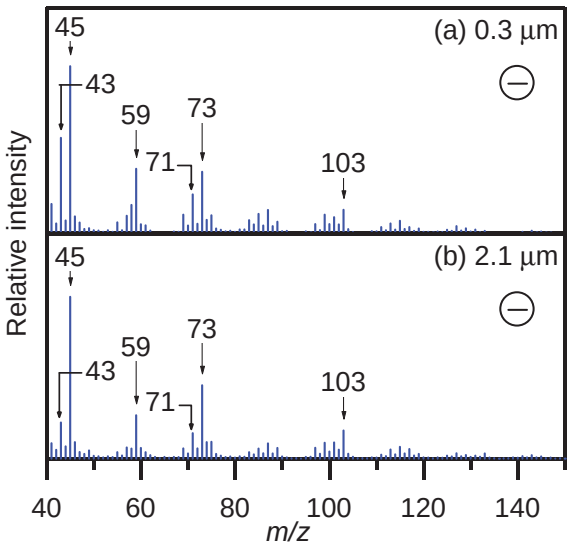

Fig. 7. Averaged negative-ion mass spectra, in which (a) the 40 smallest particles were averaged, and their mean diameter was 0.3 μm, and (b) the 40 largest particles were averaged, and their mean diameter was 2.1 μm. Data obtained from all experiment (Run Nos. 1–4) were combined and averaged.

The signal intensity (peak area) ratios of the negative ions (45/43 and 73/71) as a function of particle size were investigated. Figure 8 shows plots of the (a) 45/43 and (b) 73/71 signal intensity ratios (mean $\pm$ 1σ) from the negative-ion mass spectra against the diameters of the SOA particles. The ratios obtained from all of the experiments (Run Nos. 1–4) were combined and averaged every forty particles in order of the particle size. Figure 8a shows that the mean values and one-standard deviations of the 45/43 intensity ratios increased as the particle size increased. The 45/43 ratios had a low value of 1.9 ± 0.8 for a particle size of 0.3 μm and a high value of 4.6 ± 3.4 for a particle size of 2.1 μm, as shown in Fig. 8a. The mean values of the 73/71 intensity ratios increased more pronouncedly as the particle size increased, whereas the one-standard deviations were almost constant, as shown in Fig. 8b. The 73/71 intensity ratios had a low value of 1.8 ± 0.8 for a particle size of 0.3 μm and a high value of 3.1 ± 0.8 for a

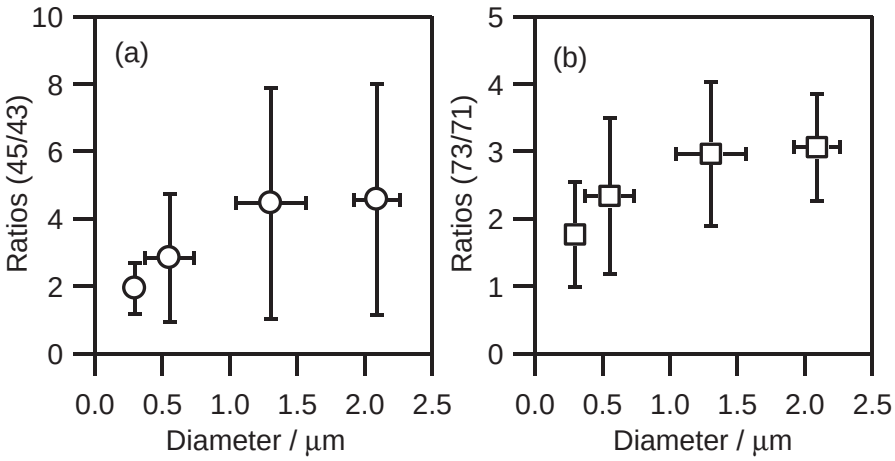

Fig. 8. Signal intensity (peak area) ratios (mean ± 1σ) of (a) $m/z = 45$ to 43 and (b) $m/z = 73$ to 71 in the negative-ion mass spectra of SOA particles formed from the CHD ozonolysis as a function of SOA particle size (mean ± 1σ), namely, PMT signal intensities. Data obtained from all experiment (Run Nos. 1–4) were combined and averaged every forty particles in order of the particle size.

particle size of 2.1 μm. It is likely that as the particle size increases, the signal intensities ($m/z = 45$ and 73) of the ions of the compounds with carboxyl groups are relatively higher than those ($m/z = 43$ and 71) of the ions of the compounds with aldehyde groups. These results suggest that the SOA particles contain more oxygenated organic compounds as the particle sizes increase; namely, the chemical compositions of the SOA particles vary as a function of the particle size.

Conclusion

In this paper, we demonstrated the applicability of the LISPA-MS technique to the study of the SOA particles formed from CHD ozonolysis. The negative-ion mass spectra of the SOA particles provided important information about the chemical compositions of the SOA particles. Mass spectral analysis of the SOA particles suggests that the second ozonolysis is rapid, that is, the products of the first ozonolysis are quickly consumed by O_3 and/or OH. In the negative-ion spectra, the intense mass peaks were explained to correspond to ions with aldehyde and carboxyl groups, which form from the reactions of CHD with O_3 and OH. The distributions of intense mass peaks in the negative-ion spectra varied as a function of the particle size. In other words, the signal intensities of the peaks ($m/z = 45$ and 73) of the ions with carboxyl groups were relatively higher than those ($m/z = 43$ and 71) of the ions with aldehyde groups as the particle size increased. This result indicates that the chemical composition of the SOA particles varies as a function of the particle size. It was demonstrated that the real-time, single-particle analysis of the SOA particles with high time-resolution by using the LISPA-MS technique is useful to investigate the formation and transformation processes of SOA particles in smog chambers.

This work was supported by SENTAN, Japan Science and Technology Agency (JST).

References

1 M. C. Jacobson, H. C. Hansson, K. J. Noone, R. J. Charlson, *Rev. Geophys.* **2000**, *38*, 267.
2 B. J. Turpin, P. Saxena, E. Andrews, *Atmos. Environ.* **2000**, *34*, 2983.
3 Y. Rudich, *Chem. Rev.* **2003**, *103*, 5097.
4 J. H. Seinfeld, J. F. Pankow, *Annu. Rev. Phys. Chem.* **2003**, *54*, 121.
5 M. Kanakidou, J. H. Seinfeld, S. N. Pandis, I. Barnes, F. J. Dentener, M. C. Facchini, R. Van Dingenen, B. Ervens, A. Nenes, C. J. Nielsen, E. Swietlicki, J. P. Putaud, Y. Balkanski, S. Fuzzi, J. Horth, G. K. Moortgat, R. Winterhalter, C. E. L. Myhre, K. Tsigaridis, E. Vignati, E. G. Stephanou, J. Wilson, *Atmos. Chem. Phys.* **2005**, *5*, 1053.
6 S. Fuzzi, M. O. Andreae, B. J. Huebert, M. Kulmala, T. C. Bond, M. Boy, S. J. Doherty, A. Guenther, M. Kanakidou, K. Kawamura, V. M. Kerminen, U. Lohmann, L. M. Russell, U. Poschl, *Atmos. Chem. Phys.* **2006**, *6*, 2017.
7 D. S. Gross, M. E. Gälli, M. Kalberer, A. S. H. Prevot, J. Dommen, M. R. Alfarra, J. Duplissy, K. Gaeggeler, A. Gascho, A. Metzger, U. Baltensperger, *Anal. Chem.* **2006**, *78*, 2130.
8 K. S. Docherty, W. Wu, Y. B. Lim, P. J. Ziemann, *Environ. Sci. Technol.* **2005**, *39*, 4049.
9 J. Liggio, S.-M. Li, J. R. Brook, C. Mihele, *Geophys. Res. Lett.* **2007**, *34*, L05814.
10 D. G. Nash, T. Baer, M. V. Johnston, *Int. J. Mass. Spectrom.* **2006**, *258*, 2.
11 D. M. Murphy, *Mass Spectrom. Rev.* **2007**, *26*, 150.
12 J. Matsumoto, K. Takahashi, Y. Matsumi, A. Yabushita, A. Shimizu, I. Matsui, N. Sugimoto, *Geophys. Res. Lett.* **2006**, *33*, L07816.
13 M. Narukawa, Y. Matsumi, J. Matsumoto, K. Takahashi, A. Yabushita, K. Sato, T. Imamura, *Anal. Sci.* **2007**, *23*, 507.
14 M. Narukawa, Y. Matsumi, K. Takahashi, A. Yabushita, *Chem. Lett.* **2007**, *36*, 904.
15 X. Zhang, K. A. Smith, D. R. Worsnop, J. Jimenez, J. T. Jayne, C. E. Kolb, *Aerosol Sci. Technol.* **2002**, *36*, 617.
16 H. Akimoto, M. Hoshino, G. Inoue, F. Sakamaki, N. Washida, M. Okuda, *Environ. Sci. Technol.* **1979**, *13*, 471.
17 K. Sato, B. Klotz, S. Hatakeyama, T. Imamura, Y. Washizu, Y. Matsumi, N. Washida, *Bull. Chem. Soc. Jpn.* **2004**, *77*, 667.
18 K. Sato, *Chem. Lett.* **2005**, *34*, 1584.
19 M. Kalberer, J. Yu, D. R. Cocker, R. C. Flagan, J. H.

Seinfeld, *Environ. Sci. Technol.* **2000**, *34*, 4894.
20 J. D. Fenske, K. T. Kuwata, K. N. Houk, S. E. Paulson, *J. Phys. Chem. A* **2000**, *104*, 7246.
21 S. Hatakeyama, T. Tanonaka, J. Weng, H. Bandow, H. Takagi, H. Akimoto, *Environ. Sci. Technol.* **1985**, *19*, 935.
22 S. Hatakeyama, M. Ohno, J. Weng, H. Takagi, H. Akimoto, *Environ. Sci. Technol.* **1987**, *21*, 52.
23 C. R. Greene, R. Atkinson, *Int. J. Chem. Kinet.* **1992**, *24*, 803.
24 J. G. Calvert, R. Atkinson, J. A. Kerr, S. Madronich, G. K. Moortgat, T. J. Wallington, G. Yarwood, *The Mechanisms of Atmospheric Oxidation of the Alkenes*, Oxford University Press, New York, **2000**.
25 H. Akimoto, F. Sakamaki, G. Inoue, M. Okuda, *Environ. Sci. Technol.* **1980**, *14*, 93.
26 F. Sakamaki, H. Akimoto, M. Okuda, *Environ. Sci. Technol.* **1981**, *15*, 665.
27 T. Ohta, *Int. J. Chem. Kinet.* **1984**, *16*, 1495.